Topology Optimization of Composite Self-Deployable Thin Shells with Cutouts

S. Ferraro * and S. Pellegrino †
California Institute of Technology, Pasadena, CA, 91125, United States

The paper presents topology optimization studies of selfs-deployable joints in thin-walled tubular structures. The joints are made entirely of ultra-thin, fiber reinforced composite materials. The objective of this research is to strategically position cutouts on the joints so that they can fold without failing, while maximizing the deployed bending stiffness. The optimal shape and position of cutouts are the results of concurrent topology optimization of these composite, thin-shell joints with geometrical non-linearities, due to their folding and self-deployable nature. Numerical methods to accurately detect failure are implemented and results from a novel level-set method for topology optimization are compared to results from classical parametric optimization and preliminary designs based on physical intuition.

Nomenclature

d	=	Representative size of composite test sample
d_b	=	Half thickness of tensile strength boundary layer
D	=	Diameter of circular cutout
E_{1f}, E_{2f}	=	Fibers Young's moduli
F_x, F_y	=	In-plane failure strengths, combination of failure coefficients and stress resultants
$F_{1t} = F_{2t}$	=	Tensile strength parameters
$F_{1c} = F_{2c}$	=	Compressive strength parameters
F_3, F_4, F_6	=	In-plane shear, bending, and twisting strength parameters
FI_1	=	In-plane failure index
FI_2	=	Bending failure index
FI_3	=	Coupled in-plane and bending failure index
f_i, f_{ij}	=	Failure coefficients, combination of strength parameters
f_r^0	=	Average tensile strength of boundary layer
K_B	=	Deployed bending stiffness of self-deployable joint

*PhD candidate, Graduate Aerospace Laboratories, 1200 East California Boulevard, Mail Code 205-45. email: sferraro@caltech.edu.
†Joyce and Kent Kresa Professor of Aeronautics and Civil Engineering, Graduate Aerospace Laboratories, 1200 East California Boulevard, Mail Code 105-05. AIAA Fellow. email: sergiop@caltech.edu.

k_c	=	Circumferential curvature
M_x, M_y, M_{xy}	=	Bending and twisting moments on a flat plate
N_x, N_y, N_{xy}	=	In-plane and shear stress resultants on a flat plate
r	=	Transition slowness parameter
R_{upper}, R_{lower}	=	Radius of curvature of upper and lower corners of joint intersection
$RP_{center}, RP_{left}, RP_{right}$	=	Reference points for boundary conditions in FE model
U_x, U_y, U_z	=	Displacements in Cartesian coordinate system
ΔM_0	=	Initial reaction bending moment from folding experiment of self-deployable joint
$\Delta\theta_0$	=	Initial folding angle from folding experiment of self-deployable joint
σ_N	=	Nominal strength of a composite laminate
$\theta_{x-RP_{center}}, \theta_{x-RP_{left}}, \theta_{x-RP_{right}}$	=	Folding angles in Cartesian coordinate system in simulation

I. Introduction

Self-deployable structures made of composite materials have several advantages over traditional deployable structures with mechanical joints. Distinctive benefits are light-weight, lower cost due to a smaller number of components, and behavior insensitive to friction. Mechanical hinges can be replaced with lighter, smaller, and cheaper continuous elements made from thin composites. Concepts for lightweight joints have already been proposed. Two examples are tape-spring rolamite (TSR) hinges [1] and compliant hinges [2]. Hinges incorporating elastic memory composites have also been shown to be a viable approach for lightweight, cost-effective mechanisms, providing controlled, low-shock deployment and structural efficiency [3, 4]. While concepts using tape-spring hinges are traditionally incorporated within straight tubes [5, 6], foldable corner joints that use the same approach have not been studied before. Progress towards composite, flexural joints must be made to replace heavier kinematic hinges and achieve a new type of self-deployable module [7] built uniquely from composite laminates. This paper focuses on a new concept for self-deployable joints [8], looking for optimization methods to find joint designs that maximize the bending stiffness of the joint in the deployed configuration while also preventing failure when the joint is folded, to allow fully-recoverable elastic folding.

The main difference between parametric and topology optimization is that in the first case, a solution to the problem under consideration, i.e. a structural design, already exists and studies are performed to explore the sensitivity of the existing solution to design variables, with the objective of improving the current design. While, in the second case, a geometry has not yet been identified and studies are performed to find a structural design numerically. Studies have been conducted on parametric optimization of composite, ultra-thin shells with geometrical nonlinearities [9, 10]. Like the present paper, these studies also aim at maximizing the deployed stiffness of the structure subject to a maximum stress

in the packaged configuration. The design variables for the optimization problem are a few geometrical features of the structure under consideration. For example, [9] optimizes the angle and width of stiffeners and the angle of slits withing thin-shell, deployable reflectors; while [10] optimizes length, width, and diameter of slots for composite tape-spring hinges. Parametric studies require a deep understanding of the mechanics of deformation of the structure and good engineering intuition to choose the geometrical features to consider.

A different approach is topology optimization, which uses adjoint sensitivity analysis and non-parametric studies [11, 12]. A review of different methodologies that use this approach was completed by Sigmund [13]. Level-set methods play an important role amongst these techniques [14]. Different studies have tackled various challenges for topology optimization. First, geometrical nonlinearities were taken into account [15–18]. Conventional topology optimization methods find the best design of a linear structure that yields the stiffest structure by minimizing the compliance. The material distribution technique is used, which assigns a numerical density to each element of a finite element discretization of the structure. Numerical density can assume a range of values between 0 (or almost 0) and 1. Based on an optimality criterion, the numerical density of each element will change during the optimization and form low-density regions, namely cutouts. The structure may deform excessively because the material becomes too sparsely distributed during optimization. In linear analysis, the excessive deformation is not a critical matter because the consequence of the analysis, i.e. deformation, is never further used. On the other hand, in nonlinear incremental analysis, the results from the previous load step are again used to proceed to the next load step. Therefore, if the previous load step yields an unrealistic deformation, the iterative solution method may have difficulty in convergence. Such convergence issues were examined by [15–18], but the examples provided only extend these successful techniques to 2-D problems, without introducing complexities such as composite materials and shell elements. The challenge of performing topology optimization using shell elements was also tackled [19, 20] as a separate issue. For example, [19] uses a commercial software, Abaqus, to perform sizing optimization of a bumper shell finite element model. This sizing optimization does not employ the material distribution technique, but creates a structure with variable thickness. Since the thickness is not allowed to reach zero value, cutouts cannot be formed on the structure. Nevertheless, [19] mentions that this is the first work that shows results for non-linear sizing of shell thicknesses using adjoint sensitivities and including the simultaneous modeling of three non-linearities: large deformations, plasticity, and contact. A different study [20] uses the level-set method, which allows for formation of cutouts, to optimize shell structures, but the examples provided do not include geometrical or material non-linearities. Finally, topology optimization problems including composite materials were analyzed [21, 22] using numerical homogenization. This technique is also used to compute composite materials' properties [23]. However, the class of composites referred to here is not the most commonly used fiber-reinforced laminates, made of orthotropic plies, but two or three-phase composites with extremal values of bulk modulus or extremal thermal expansion behavior. Furthermore, these studies only focus on optimizing the material composition of a structure, without including other types of non-linearities.

This paper aims at filling the gap the previously mentioned optimization techniques have left, which is the concurrent topology optimization of composite, thin-shell structures with geometrical non-linearities. A novel approach to optimization of self-deployable joints, using a level-set method, is presented. The goal is to find a joint design that is stiff when deployed, compliant during folding (to avoid failure), ultra-lightweight, and self-deployable. The advantageous strategy of outsourcing the finite element formulation part of the optimization analysis to a commercial software [24], i.e. Abaqus, is also employed. Three main challenges for the optimization problem were identified: first, geometrical nonlinearities due to the self-deployable nature of the joint; second, ultra-thin shells; third, composite materials. Miter joints, made entirely of thin composite materials, were designed, simulated, built, and tested. The joints fold up to 45 degrees (or more in some cases), hence undergoing large displacements. Geometrical non-linearities deriving from large displacements were studied using finite element analysis. While linear elastic formulation was used to simulate the material behavior, material tests were performed to characterize the strength of the composite and introduce a failure criterion in the numerical simulations. Before performing optimization studies, preliminary designs based on literature review and physical intuition were explored. A joint design capable of folding without failing was found, but the bending stiffness was greatly reduced because of the size of the cutout. Henceforth, parametric and topology optimization studies were performed to find new cutouts. The paper presents techniques used to perform these optimization studies and the results achieved. Experimental results on composite joints, folded to 45 degrees, with cutouts derived from the optimization studies are also presented. Finally, different designs are compared in terms of deployed bending stiffness and norm of the most critical failure index.

II. Joint Design

Fiber-Reinforced-Polymers (FRP) self-deployable joints for in-plane deployment mechanisms were chosen as a case study. The chosen shape is a miter joint, where two thin-walled tubes intersect at 90 degrees, Fig. 1. The joints must fold, with the two tubes rotating towards each other. The total folding angle is the sum of the folding angles of the two tubes. Thin-walled tubular joints were studied with the intent of providing a new, lighter option for building deployable modules [7] that can be assembled into very large ($>$ 10 m diameter) space structures. Each joint within these kind of modules connects at least four tubes, while this paper focuses on miter joints, which connect only two tubes. Miter joints were chosen because their straightforward shape provides a good starting point for understanding and resolving some of the design challenges. For example, because of manufacturing tolerances, the tubes of the deployable modules can have slightly different lengths than the ones specified by design. This creates internal stresses when the tubes are assembled into a module. Hence, sharp intersections at the joints are desired to avoid a bending dominated structure and preserve shape accuracy. Nevertheless, the joints must be able to fold without failing, but sharp corners produce stress concentration. It follows that one of the design challenges is to identify values of the radius of curvature at the intersection between tubes that allow the joint to fold without failing, while preventing a bending dominated structure.

Finite element simulations of miter joints, discussed in the next section, were useful to understand how these joints deform while folding and where stress concentrates, thus allowing to identify areas where to place cutouts. Although a miter joint is simpler than joints with more than two intersecting tubes, this shape gives the geometrical complication of non-zero Gaussian curvature at the intersection of the two tubes. Topology optimization studies discussed in this paper aim at generalizing the process of placing cutouts on these type of joints in order to progress towards joints with more intersecting tubes.

Plain-weave, quartz fiber composites were chosen because of their higher ultimate strain, measured at 2.6 % , compared to carbon fiber composites, which is useful to fold the joint. Considering that the 0 degrees direction of the fibers corresponds to the axial direction of each tube, the layup is composed of four regions of two, three, four and six plies respectively, as shown in Fig. 1. The plies are oriented as follows: two-ply regions [45/45], three-ply regions [45/0/45], four-ply regions [45/45/45/45], and six-ply regions [45/45/0/0/45/45], where 0 and 45 indicate plain weave laminae consisting of fibers oriented respectively at 0/90 degrees and +45/-45 degrees. This particular layup was taken from previous studies [8].

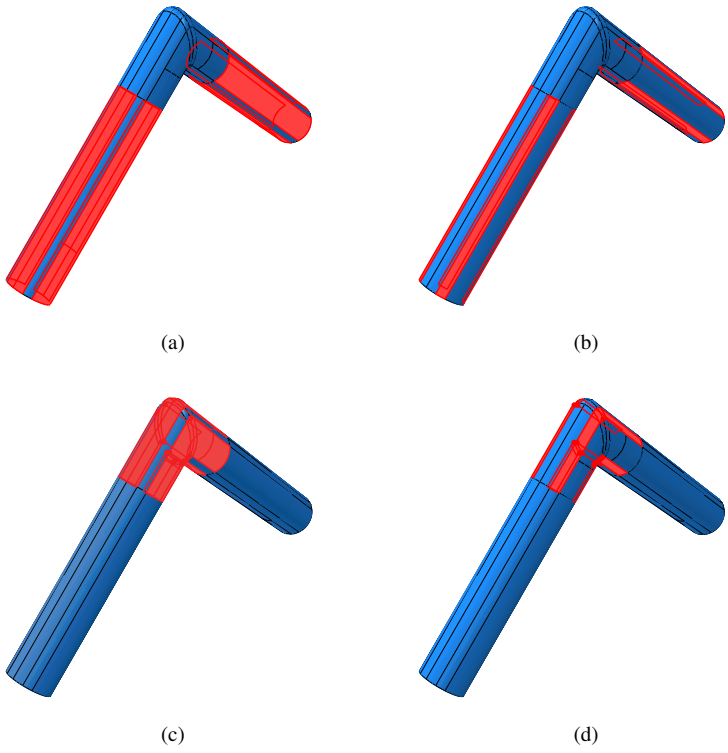

Fig. 1 Regions with different laminates (a) 3 plies, (b) 6 plies, (c) 2 plies, (d) 4 plies.

III. Analysis Techniques

Two techniques were adopted to study the miter joints. First, a finite element model to analyze the folding behavior of thin-shell structures. Second, a failure criterion for thin, plain-weave, FRP laminates to numerically detect failure of the joints. These techniques were used to improve the initial design.

A. Finite Element Model

In order to characterize the folding behavior of the joints, large-displacement simulations, with linear-elastic material, were carried out with finite element software. The model was built in Abaqus 2017 with S3 shell elements. The four different layups described before were defined in the model, using a feature provided in Abaqus and called "general section properties". The feature allows to manually input the ABD stiffness matrix of a composite material and it was used to match the bending stiffness matrix of each layup, obtained from 4-point bending experiments.

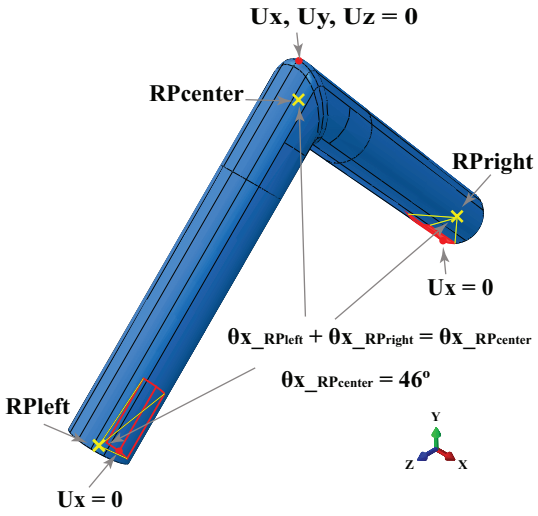

Fig. 2 Finite element model and boundary conditions.

Figure 2 shows the boundary conditions applied to the finite element model. Three massless reference points, RP_{center}, RP_{left}, and RP_{right}, were defined. Two rectangular patches, shown in red, were coupled to the left and right reference points such that the in-plane rotations of the patches, θ_x, match the rotation imposed to the reference points. The rotations of the three points are coupled so that the sum of the rotations of the left and right reference points equals the rotation of the center one, which is set at 45 degrees. Finally, two nodes at the bottom of the joint, shown by red dots in Fig. 2, are constrained to remain in the y-z plane and all the translations of the node at the top are set to zero. These boundary conditions make the joint fold by 45 degrees and allow each tube to fold independently of the other, without constraining possible non-symmetric folding. The simulations are carried out with an implicit solver, where after each increment the analysis starts Newton-Raphson iterations to enforce equilibrium of the internal forces with the external loads.

B. Failure Criterion

A laminate failure criterion [25], suitable for ultra-thin, plain-weave composites, was used to predict failure of the joints. The criterion uses three non-dimensional failure indices to capture the in-plane, bending, and coupled in-plane and bending failure, defined as follows:

$$FI_1 = f_1(N_x + N_y) + f_{11}(N_x^2 + N_y^2) + f_{12}N_xN_y + f_{33}N_{xy}^2 < 1 \tag{1}$$

$$FI_2 = f_{44} \times max(M_x^2, M_y^2) + f_{66}M_{xy}^2 < 1 \tag{2}$$

$$FI_3 = max\left(\frac{N_x}{F_x}, \frac{N_y}{F_y}\right) + \frac{max(|M_x|, |M_y|)}{F_4} < 1 \tag{3}$$

The failure coefficients, f_i and f_{ij}, are a combination of physical strength parameters. Five strength parameters were measured or calculated and are shown in Tables 1 and 2. To obtain a conservative analysis, the lowest values of the strength parameters were used in the failure criterion. For both tensile and compressive strengths, $F_{1t} = F_{2t}$ and $F_{1c} = F_{2c}$, the subscripts 1 and 2 refer to the directions parallel and perpendicular to the fibers respectively. The compressive strength was calculated using a plastic fiber microbuckling criterion [26]. The strength parameters F_3, F_4, and F_6 represent in-plane shear, bending, and twisting strength of the material.

Table 1 Material strength parameters for two-ply laminates of Astroquartz fibers and cyanate ester resin.

Strength Parameter	Lowest Value	Number of Test Samples	Average Value	Population SD
$F_{1t} = F_{2t}$ [N/mm]	71.30	5	74.89	2.83
$F_{1c} = F_{2c}$ [N/mm]	18.19	-	-	-
F_3 [N/mm]	4.73	5	4.95	0.27
F_4 [N]	2.98	4	3.26	0.28
F_6 [N]	1.00	4	1.10	0.06

Table 2 Material strength parameters for four-ply laminates of Astroquartz fibers and cyanate ester resin.

Strength Parameter	Lowest Value	Number of Test Samples	Average Value	Population SD
$F_{1t} = F_{2t}$ [N/mm]	148.85	3	150	1.47
$F_{1c} = F_{2c}$ [N/mm]	54.87	-	-	-
F_3 [N/mm]	14.27	5	15.44	1.07
F_4 [N]	6.84	4	8.78	1.28
F_6 [N]	3.49	4	3.65	0.10

The criterion applies only to layups with same-orientation plies. Therefore, only regions with two and four plies can be analyzed, since all the plies are oriented at ± 45 degrees. This limitation is acceptable because experimental results [8] showed that failure occurs at the joint intersection, where the regions with two and four plies are located. The failure criterion was used to extend the simulations based on linear elastic material and predict failure of the joints in order to improve their design. The three failure indices were calculated at each step of the simulations and contour plots were obtained. As an example, a joint with a circular cutout was analyzed and it is shown in Fig. 3. According to the failure criterion, when any failure index, calculated on each element of a finite element mesh of the structure, exceeds the value of 1 the element has failed. The black areas plotted in Fig. 3 are regions where the first failure index is smaller than 1. The white areas are regions that were not examined. Finally, all the elements plotted with a color other than white or black have reached a failure index greater than 1. For all the cases examined in this study, if a joint fails it will fail in the two-ply region and the first failure index FI_1 is the most critical. Therefore, this study will only examine FI_1.

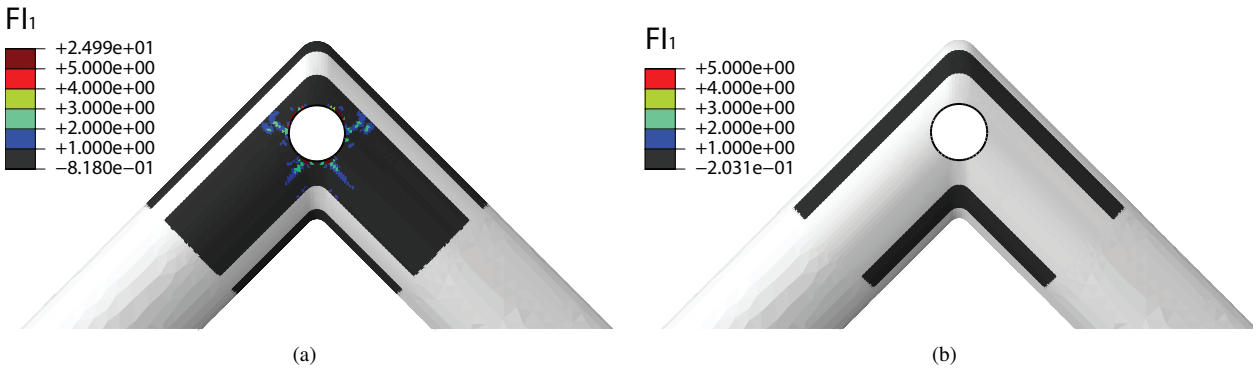

Fig. 3 Contour plots of in-plane failure index FI_1 corresponding to a folded joint, plotted on a deployed joint (a) region with 2 plies, (b) region with 4 plies.

IV. Preliminary Designs Based on Literature Review and Physical Intuition

The first miter joints considered as a case study [8] have sharp corners at the intersection between the two tubes, as shown in Fig. 4(a). An initial attempt to the design of cutouts was guided by the results obtained from the finite element analysis in Section III.A and preliminary folding experiments. When the joint is folded, with the same boundary conditions described in III.A, the deformation along the tubes transitions from a longitudinal ovalization of the cross section at the base of the joint to a transverse flattening of the cross section at the intersection between the two cylindrical surfaces. The base of the joint is where the boundary conditions are applied and it is 20 cm away from the intersection. The transverse flattening creates regions of localized curvature. A contour plot of circumferential curvature k_c is shown in Fig. 4(a). The stress distribution in the joint can be reduced by simply placing cutouts where localized curvature develops. For this reason, all the designs have at least one cutout on each side of the joint, where the two cylindrical tubes intersect. The first design was obtained by placing circular cutouts, of diameter D = 14 mm, centered on the region of highest localized curvature, Fig. 4(a).

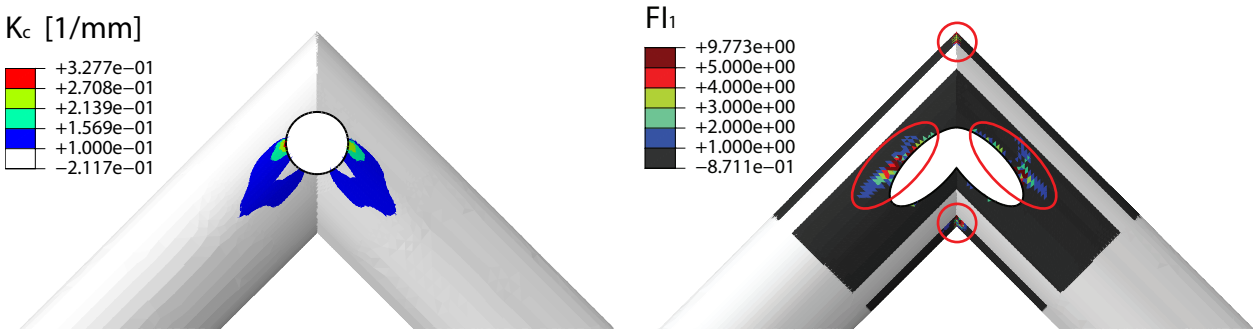

Fig. 4 Miter joints with sharp corners (a) contour plot of circumferential curvature on joint with circular cutout with D = 14 mm, (b) contour plot of FI_1 on joint with cutout made of intersecting ellipses.

A second class of cutout shapes, Fig. 4(b), was obtained by intersecting two ellipses and symmetrically varying the major and minor axes of each ellipse. Elliptical cutouts were chosen to eliminate areas of the joint where highest curvature changes occur, according to the finite element analysis. A result from the study on elliptical cutouts is presented in Fig. 4(b). The areas on the joint with $FI_1 > 1$ are circled in red. It is clear that elliptical cutouts do not prevent large areas of the joint from failing. First, failure occurs at the sides of the cutout, where a hinge-line naturally forms when the joint is folded. Second, failure also occurs at the sharp intersection corners. Two studies were carried out to prevent failure in both regions. First, the intersection with sharp corners was replaced with a smooth intersection, shown in Fig. 3. Design studies were performed on the radius of curvature of the upper corner, R_{upper}, and lower corner, R_{lower}, of the joint intersection [8]. Values of R_{upper} = 5 mm and R_{lower} = 3 mm were chosen as the smallest radii needed to avoid failure at the corners and prevent a bending dominated structure. Second, a topology optimization study was carried out, as described in the next section.

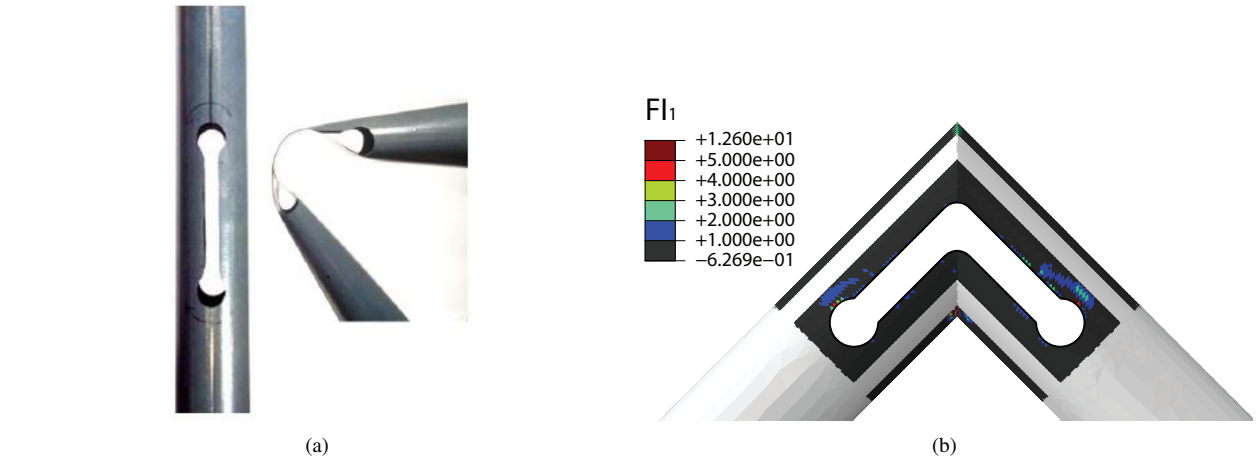

Fig. 5 Engineering designs inspired by literature review [5, 10] (a) example of tape spring hinge, (b) contour plot of FI_1 on joint with cutout inspired by tape spring hinges.

The cutout shape in Fig. 5(b) was an adaptation of designs previously developed for thin-shell, cylindrical booms with slotted hinges [5, 10]. An L-shaped cutout was created to follow the shape of the joint and circular ends were placed at both ends of the cutout to prevent crack formation. A contour plot of the first failure index, Fig. 5(b), shows that this kind of shape does not prevent failure of the joint. Although there are only localized areas on the joint that reach the highest values of first failure index, FI_1, large areas on the joint do not satisfy the failure criterion. Since the cutout shapes examined so far did not prevent failure of the joint, larger cutouts where explored. In particular, a successful design, shown in Fig. 6, was found by partially removing the two-ply region. Hinge-lines formed at both ends of the cutout, Fig. 6(b), thus allowing the joint to fold much more than 45 degrees without failing. Partially removing the two-ply region of the joint resolved the issue of material failure, but greatly reduced the bending stiffness of the joint if compared to other cutout shapes. Table 3 and Fig. 18 provide a summary of results for bending stiffness and norm of first failure index.

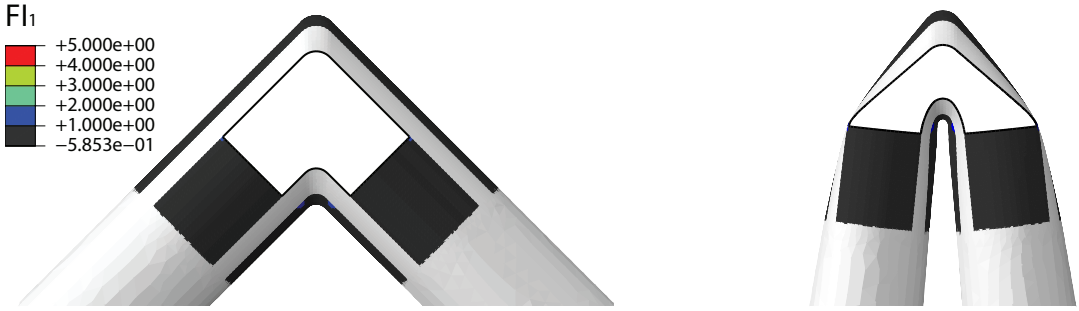

Fig. 6 Successful shape with smooth joint intersection and partially removed two-ply region (a) contour plot of FI_1 on deployed shape (b) contour plot of FI_1 on folded shape.

V. Optimization Problem Formulation

The objective of the optimization studies was to search automatically for non-intuitive solutions. In particular, the problem of finding a better shape, number, and position of cutouts to fulfill stiffness requirements and failure constraints on a self-deployable joint was studied. The minimization problem is defined as:

$$\min_{x_1 \ldots x_n} \left[\frac{\|FI_1\|_2}{\|FI_1\|_{2-in}} - \frac{K_B}{K_{B-in}} \right] \qquad subject\ to\ \ \alpha_i < x_i < \beta_i, \ \ i = 1, 2, 3, ..., n \tag{4}$$

It was decided not to study a minimization problem where the first failure index must remain smaller than 1, but to minimize the norm of the failure index at each consecutive folding step, while maximizing the bending stiffness of the deployed joint. This approach allowed to find a solution in cases that would have otherwise been over-constrained. The objective function in Eq. (4) is a linear superposition of two terms. The first term is the Frobenius norm of the

first failure index, calculated at each folding step of the joint and normalized with respect to the same norm for the initial guess design. The second term is the bending stiffness of the joint in the deployed configuration, normalized with respect to the bending stiffness of the initial guess design. Note that in the first iteration of the optimization algorithm the objective function equals zero.

Two optimization approaches are presented. The first, applies a parametric optimization technique, and the second uses a level-set method for topology optimization. The parametric optimization was performed to generate a baseline to assess the results of the level-set method and to provide a comparison. The initial guess is shown in Fig. 3. Circular cutouts with diameter D = 14 mm were placed in regions of localized curvature.

VI. Parametric Optimization of Single Cutout

The parametric optimization approach falls within classical optimization methods. The cutouts could be placed anywhere on the joint, but the finite element simulations showed that stress concentrates at the intersection between the two cylindrical surfaces. Since the joint is symmetric, two identical cutouts were placed on each side of it, thus reducing the problem to studying the shape of a single cutout. Instead of placing the cutouts directly on the surface of the joint, a projection plane, shown by blue lines in Fig. 7, was created on the side of the joint. This technique allowed to simplify the 3-D problem into a 2-D one. A contour was defined on the projection plane using control points and a cubic spline fit between all the points (spline function defined in Abaqus 2017). The contour was then projected onto the thin-shell joint. The coordinates of each control point, x_i, on the projection plane were chosen as design variables of the minimization problem.

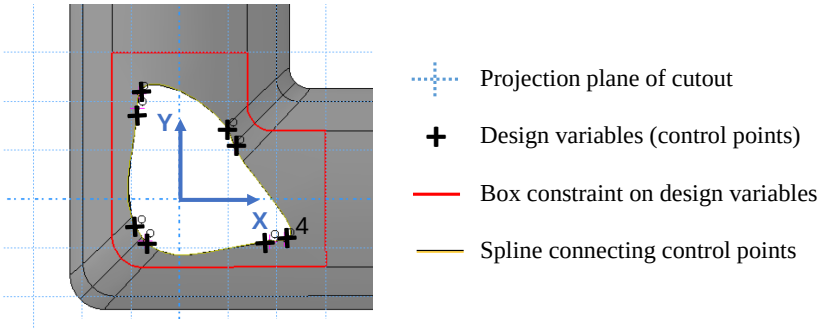

Fig. 7 Description of design space for parametric optimization of single cutout.

The inequality constraints in Eq. (4) were defined so that the control points remain within the red contour, Fig. 7, corresponding to the cutout in Fig. 6, which allowed the joint to fold without failing. Constraining the control points to fit within this contour not only ensures that the cutout will remain within the physical boundaries of the joint, but it also limits the design space to shapes that have a smaller area than the one already found, Fig. 6, thus improving the possibility of finding solutions with higher bending stiffness.

A. Objective Function Studies

Trend studies of the Frobenius norm of the first failure index, plotted against one of the design variables in Fig. 8, show that the problem under consideration is non-convex. Each data point in Fig 8 was obtained by running a finite element simulation of a joint that folds. Each one of these joints has a slightly different shape of cutout, given by the value assigned to the design variable under consideration. Data points were interpolated with a line, which shows a noisy function. If the function is smoothened, red line in Fig 8, one can focus on the general trend, instead of the noise, which shows a non-convex behavior.

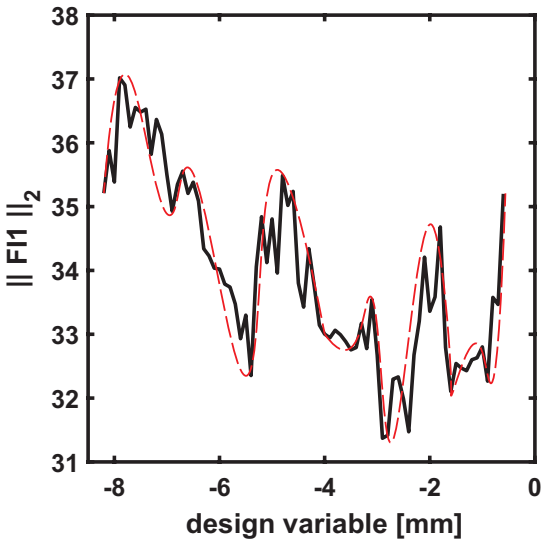

Fig. 8 Frobenius norm of first failure index plotted against a design variable.

A global search method that does not utilize gradient information was implemented. The Basin-Hopping algorithm [27] was chosen for global optimization. Basin-Hopping is a stochastic, two-phase method that combines a global stepping algorithm with local minimization at each step. The algorithm iterates by first, performing random perturbation of design variables, second, performing local optimization, and third, accepting or rejecting new design variables based on an acceptance test. The acceptance test used here is the Metropolis criterion of standard Monte Carlo algorithms [28], although there are many other possibilities. Local minimization was performed with Constrained Optimization BY Linear Approximation (COBYLA) [29], an optimization algorithm for constrained problems where the derivative of the objective function is not known. During an iteration, a linear approximation of the objective function is solved to obtain a candidate for the optimal solution. The candidate solution is evaluated using the original objective and constraint functions, yielding a new data point in the optimization space. This information is used to improve the linear approximation used for the next iteration of the algorithm. When the solution cannot be improved anymore, the step size is reduced, refining the search. When the step size becomes sufficiently small, the algorithm finishes. The Basin-Hopping and COBYLA algorithms were taken from publicly available libraries for Python scripts and

incorporated within the parametric optimization method. A Python script generates an input file for Abaqus 2017, with a chosen cutout shape for the joint, hence assigned design variables. Abaqus software runs a finite element analysis of the prescribed joint design and returns values of first failure index and bending stiffness. The script evaluates the objective function and calls the Basin-Hopping and COBYLA algorithms to update the design variables. Each set of design variables defines a new cutout shape, and therefore a new joint design, which is generated and passed to Abaqus for another finite element analysis. Optimization loops continue to run until the maximum number of iterations allowed is reached. The objective function, norm of the first failure index, and bending stiffness at each iteration of the optimization study are plotted in Fig. 9. The objective function reaches a steady state after 400 iterations.

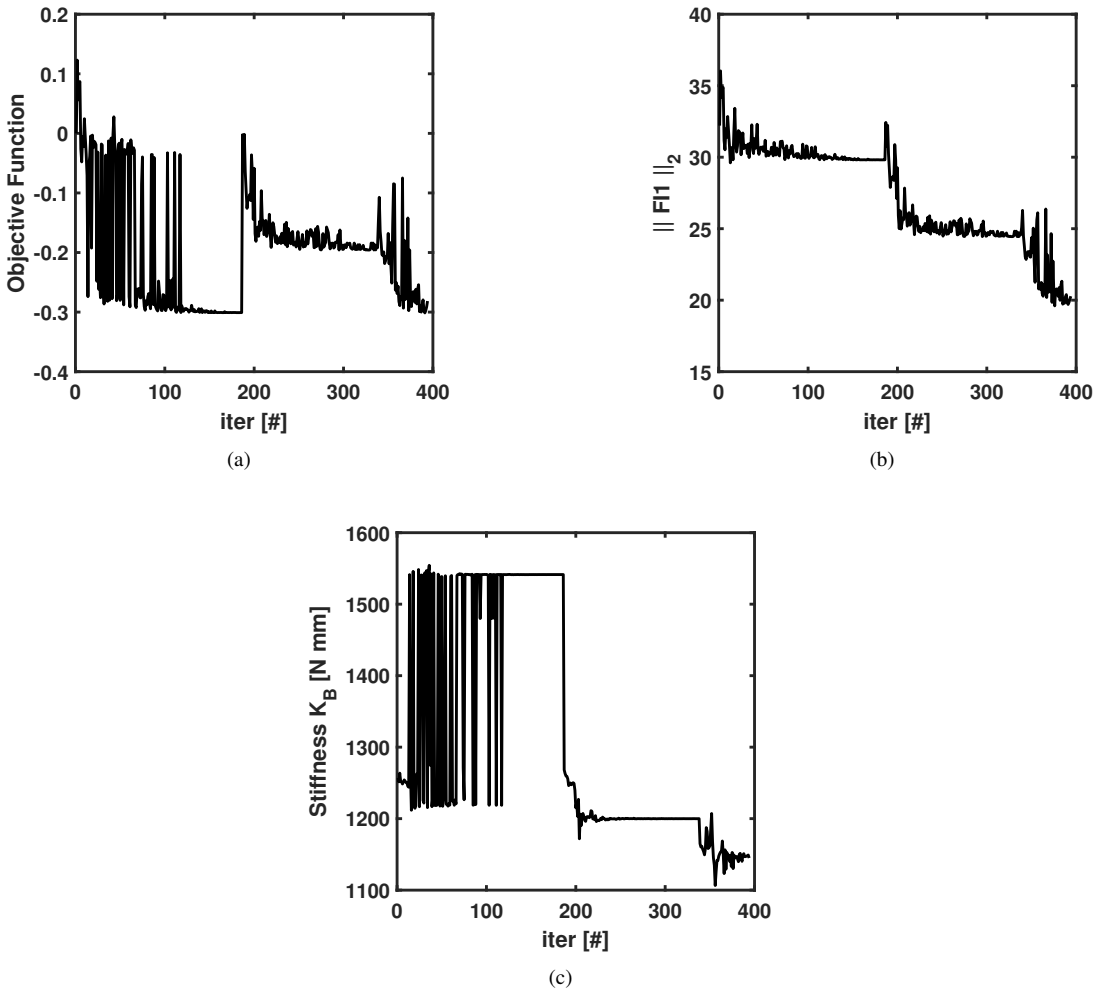

Fig. 9 Plots from Basin-Hopping algorithm (a) objective function, (b) Frobenius norm of first failure index, (c) bending stiffness.

B. Results from Parametric Optimization

The optimized shape of the cutout is shown in Fig. 10. The resulting bending stiffness and norm of first failure index are shown in Fig. 9 and are 1148 [Nmm] and 19.7 respectively. Although the control points that define the cutout are constrained to remain within the red contour shown in Fig 7, which only spans through a region with 2 plies, there are no constraints on the cubic spline function that connects these points. In fact, the cutout resulting from the parametric optimization overflows into a region with 4 plies, thus reducing the bending stiffness of the joint. On the other hand, it is clear that this cutout has significantly reduced the areas on the joint that do not satisfy the failure criterion, compared to the baseline design in Fig. 3. It has also lowered the maximum value of the first failure index, which reaches peaks of value 4 for a few, small elements surrounding the cutout, while a few more elements reach values of 1 or 2. This result represents a shift from a global failure of the joint to a local failure. Further discussion of this result is provided in Section IX.

The one drawback of this method is that it requires a significant number of design variables; in this case, more than 10 control points and therefore 20 design variables. If two cutouts were considered, instead of a single one, the number of design variables would be more than doubled (considering the position of the two cutouts as additional degrees of freedom for the optimization problem). It is reasonable to conclude that parametric optimization of composite, thin-shells undergoing large displacements can be computationally expensive and needs to deal with the complexity of having a large number of design variables.

Fig. 10 Contour plot of FI_1 on joint resulting from parametric optimization of single cutout (a) two-ply region, (b) enlarged image of a few elements that do not satisfy the failure criterion.

VII. Optimization with Level-Set Method

A novel approach to topology optimization using a level-set method was studied. This method has the advantage of drastically reducing the number of design variables when compared to the previous approach, based on parametric description of the contour of each cutout. It also allows for broader exploration of shapes, number and position of cutouts using only a few design variables. The implementation of the method is very similar to the one described for

the parametric optimization approach. A Python script assigns values to the design variables under consideration and calls a Matlab script to generate new shapes of cutouts, based on the assigned design variables. Once these shapes are created, the Python script generates an input file for Abaqus 2017, with each new joint design, which runs a finite element analysis and returns the values of the first failure index and of the bending stiffness.

A. Method Description

The minimization problem is still defined by Eq. (4), but the inequality constraints are replaced by the function definition and the design variables are different from the ones considered in the parametric optimization method. The general idea of the level-set method is to utilize some 3-D basis function, $z = f(x, y)$, defined on the same projection plane used for the parametric optimization approach. The basis function vanishes at the boundaries of its domain. This eliminates the need for introducing constraints to keep the cutout projections within the physical boundaries of the joint, since the constraints are automatically satisfied by the basis function. A cutting plane, parallel to the x-y plane, is then introduced such that contour shapes are formed. The z-coordinate of the plane directly influences the contour shapes that are generated through the intersection of the plane and the chosen basis function.

The method is divided into three main steps, shown in Fig. 11. The first step, Fig. 11(a), requires finding a conformal mapping between a convenient domain on which the basis function is described (in this case a square was chosen) and the domain that will serve as projection plane for the cutouts. The latter was chosen as an L-shaped, smooth domain that represents a portion of the side view of the joint. The second step, Fig. 11(b), involves choosing a basis function and applying the conformal mapping to it. Two basis functions were investigated, a series of cosines squared:

$$z = \sum_{h=1}^{N_h} \sum_{l=1}^{N_l} a_n \left[\cos\left(2h+1\right)\frac{\pi x}{2} \times \cos\left(2l+1\right)\frac{\pi y}{2} \right]^2, n = 1, 2, 3, ..., N_h N_l \tag{5}$$

and a series of cosines and sines squared:

$$z = \sum_{h=1}^{N_h} \sum_{l=1}^{N_l} a_n \left[\left(\cos\left(2h+1\right)\frac{\pi x}{2} + \sin\left(h\pi x\right) \right) \times \left(\cos\left(2l+1\right)\frac{\pi y}{2} + \sin\left(l\pi y\right) \right) \right]^2, n = 1, 2, 3, ..., N_h N_l \tag{6}$$

Both functions vanish on a square bounded between -1 and 1 on both the x-axis and the y-axis. The third step, Fig. 11(c), requires intersecting the chosen basis function, Eq. (5) or Eq. (6), with a plane parallel to the x-y plane. Examples of shapes of cutouts that can be obtained on both initial and mapped domains are shown in Fig. 11(c).

Once the basis function is chosen, the only design variables used to define the problem and run the optimization analysis are the z-coordinate at which the cutting plane is set, $z = c$, and the numbers of terms in the series, N_h and N_l, which define how many peaks the function will have, thus defining the number of cutouts. In this study, the coefficients of the series, a_n, where chosen equal to 1, because a_n is a dual variable of the z-coordinate. If the height of the function, hence a_n, is fixed, the z-coordinate spans the whole function thus generating different shapes, size and number of

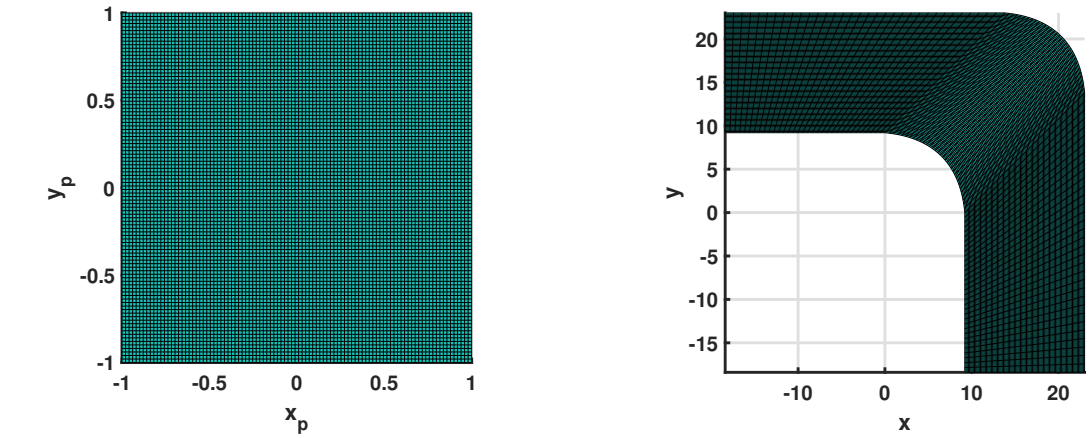

(a)

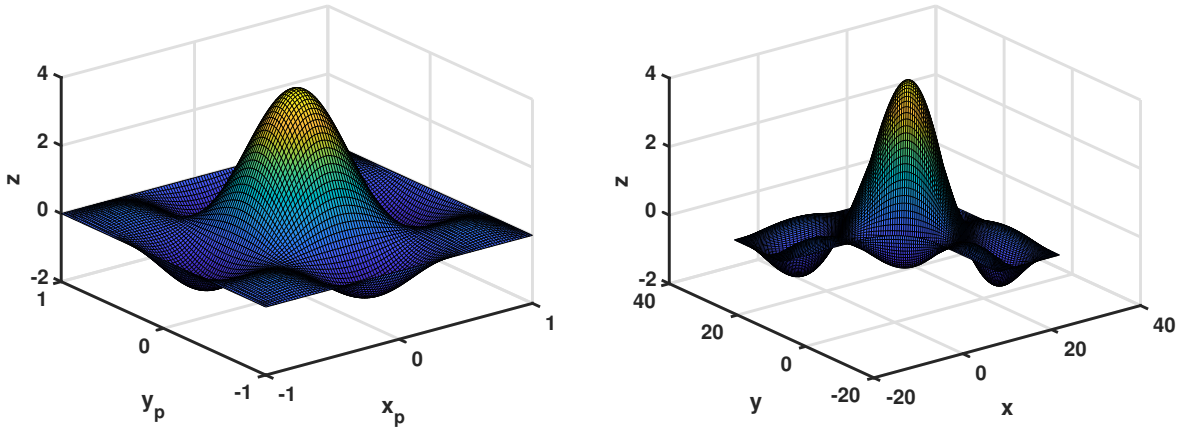

(b)

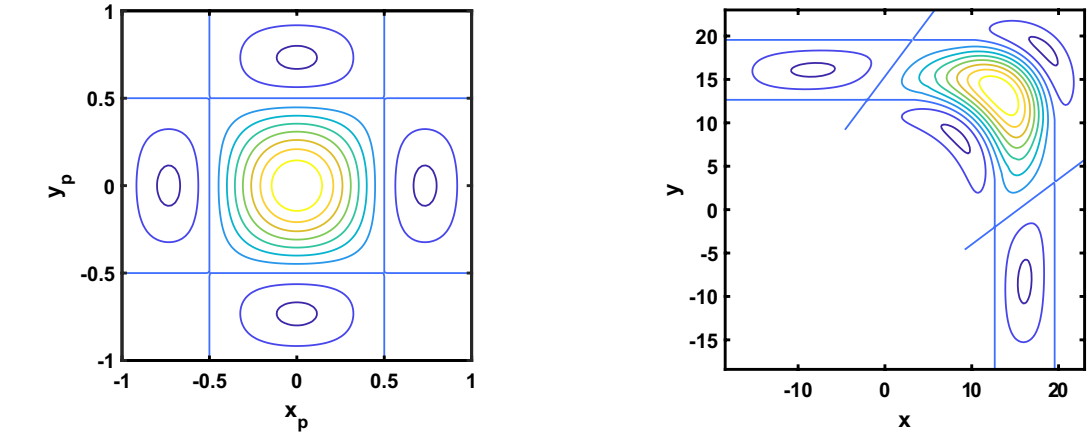

(c)

Fig. 11 Three steps of level-set method (a) define conformal mapping, (b) choose set of basis function and apply conformal mapping, (c) cut function at z = constant.

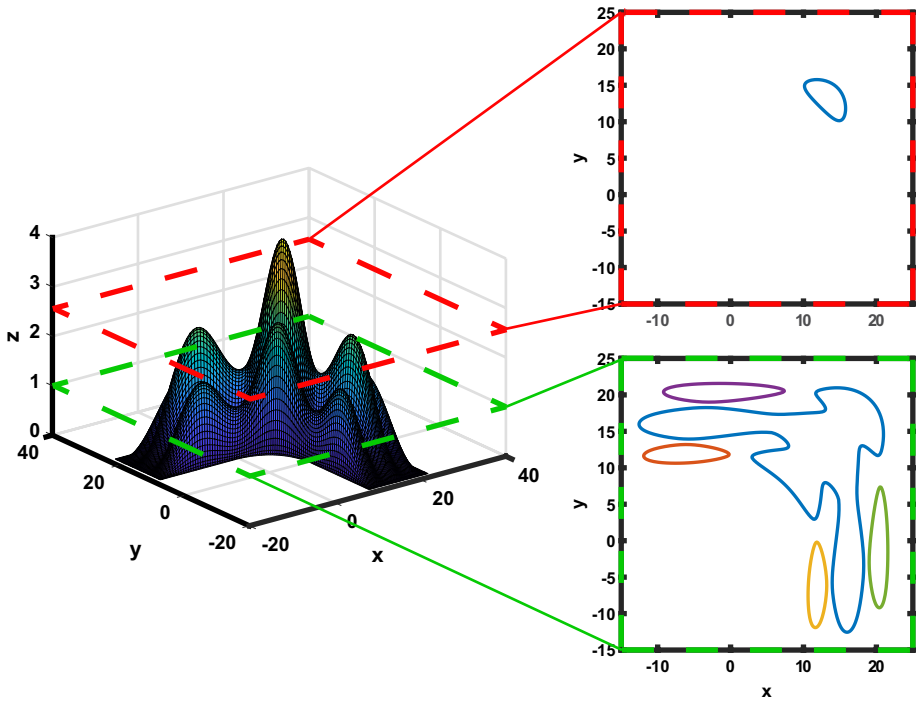

Fig. 12 Examples of cutout shapes obtained by intersecting a chosen basis function with planes.

cutouts. On the other hand, if the z-coordinate is fixed, the same cutouts can be generated by varying the height of the basis function. Additionally, the inclination angles between the cutting plane and the x-y plane could also be chosen as design variables to generate an even wider range of shapes.

B. Results from Level-Set Method

Three examples of joint designs generated using the level-set optimization approach are shown in Figs. 13 - 15. The first design, Fig. 13, was obtained using a series of cosines squared, Eq. (5), and hence, the shapes of the cutouts are symmetric. This design produced the lowest value of the cost function, and was obtained for the choice $N_h = 0$ and $N_l = 2$. The boomerang-shaped cutouts leave strips of material connecting the right and left parts of the joint, thus providing additional bending stiffness. As for the resulting shape from the parametric optimization studies, this joint design also fails in localized areas. The second design, Fig. 14, was again obtained using a series of cosines squared, but choosing $N_h = 1$ and $N_l = 2$. This topology uses a mechanism similar to the previous one to increase bending stiffness and limit failure. The three cutouts at the center remove areas of localized curvature change, while keeping a few strips of material connecting the right and left parts of the joint. In this configuration, two thin slits on the sides help releasing stress when the join folds. Finally, the third design, Fig. 15 , was obtained using a series of cosines and sines squared, Eq. (6), thus resulting in a non-symmetric distribution of cutouts. Given the results from the parametric optimization, non-symmetric cutouts were studied as a viable solution to the optimization problem. The shape in Fig. 15 was obtained choosing $N_h = 2$ and $N_l = 0$. Despite being the best result obtained using a non-symmetric basis function, this design fails on a larger

area when compared to the other two designs obtained with the level-set method. A summary of bending stiffness and norm of first failure index values for these three designs is provided Table 3 and in Fig. 18

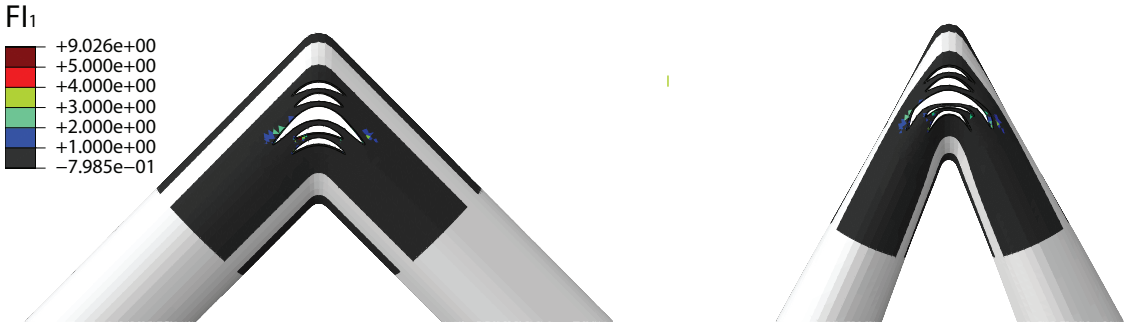

Fig. 13 Contour plot of FI_1 on joint obtained with level-set method using Eq. (5) and N_h=0, N_l=2.

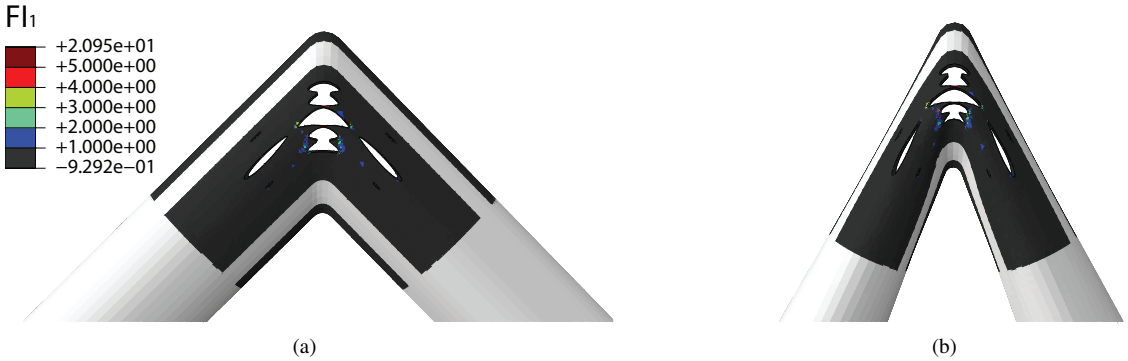

Fig. 14 Contour plot of FI_1 on joint obtained with level-set method using Eq. (5) and N_h=1, N_l=2.

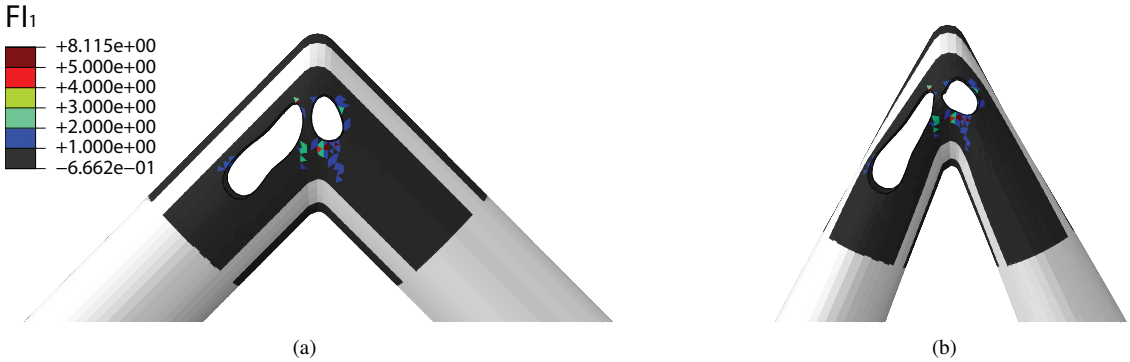

Fig. 15 Contour plot of FI_1 on joint obtained with level-set method using Eq. (6) and N_h=2, N_l=0.

C. Experimental Verification of Level-Set Method Results

To experimentally verify the results from the level-set optimization method, a self-deployable joint was built and the cutouts in Fig 13 were laser-cut. Thin, pre-impregnated fabrics were used. In particular, plain-weave 525

Astroquartz II fabric (quartz fiber), from JPS Composite Materials, and PMT-F6 cyanate ester resin, from Patz Materials & Technologies. The fibers Young's modulus is $E_{1f} = E_{2f} = 72$ GPa. Each ply has a measured thickness of 90 μm and areal density of 105 gsm. Each tube of the joint has a circular cross section with diameter of 31.8 mm. The joint was built using a silicone molding manufacturing technique [8]. One ply of the layup was cut into four geometric patterns and assembled directly on the silicone mold, thus creating overlapping strips of material along the axial direction of each shaft. Subsequent plies were assembled following an identical procedure. A cure in autoclave at elevated pressure, 551.6 KPa, and temperature, 180 °C, was used to complete the manufacturing process. This layup arrangement was designed to overcome the complications of the non-zero Gaussian curvature at the joint between the two cylindrical surfaces.

A quasi-static folding experiment was carried out using the setup shown in Fig. 16(a). Two 35 mm × 15 mm, curved clamps that conformed to the curvature of the cylindrical tubes were used. The clamps constrained a small region at the end of each tube, thus leaving the end cross-sections free to ovalize. They also connected the tubes to brackets that were initially aligned at 45 degrees, to mount the joint. The experiment was rotation controlled and the rotations were imposed manually. One of the brackets was mounted on ball bearings and it was free to slide towards the other. The brackets were mounted on gearboxes, connected to strain gauges and a data acquisition system. Once the sliding bracket was rotated, the reaction moment from the tube connected to that bracket was recorded. The second, fixed bracket was then rotated until the reaction moment recorded on the attached tube equaled the one recorded on the other tube. This process was repeated until the joint was folded to 45 degrees, with rotation increments between 1-3 degrees. The same displacement and loading conditions were applied in the numerical simulations.

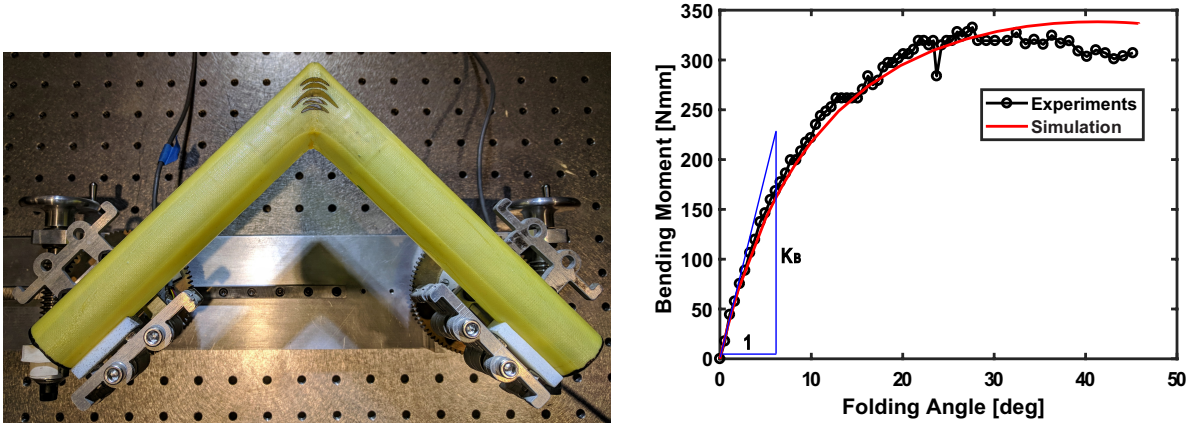

(a) (b)

Fig. 16 Folding experiment (a) setup, (b) test data compared to simulation results. The graph shows the reaction bending moments plotted against the folding angle; 0 deg corresponds to a fully deployed joint and the angle grows as the two tubes rotate towards each other.

At the end of the test, the moment-rotation profile was obtained by plotting the folding angle and the corresponding moment at each step, Fig. 16(b). The moment-rotation profile resulting from numerical simulations was then superposed

to the experimental one to validate the results. The two curves show good agreement in the first 30 degrees of folding angle, but deviate from each other for the last 15 degrees, possibly due to manufacturing imperfections of the physical joint and to the fact that the simulation was built using a linear-elastic description of the composite material, without accounting for imperfections.

Two results stand out from this experiment. First, the bending stiffness predicted by the simulation perfectly matches the bending stiffness of the joint in the deployed configuration, defined by the tangent at the origin of the moment-rotation curve as follows:

$$K_B = \frac{\Delta M_0}{\Delta \theta_0} \left[\frac{Nmm}{rad} \right] \tag{7}$$

Second, the joint does not suffer global failure when folded. This means that the joint does not develop any visible cracks and that the deployed bending stiffness, experimentally measured via moment-rotation curve, does not change before and after the joint has been folded.

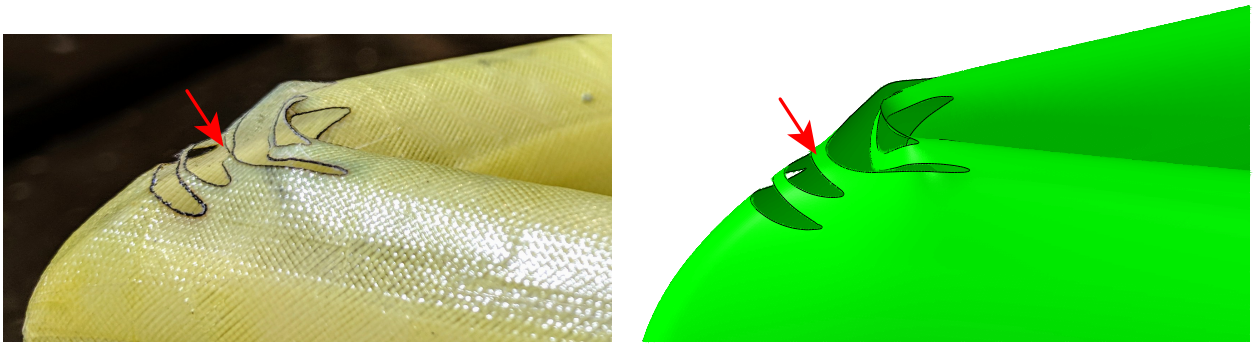

(a) (b)

Fig. 17 Deformed shape of the joint near the cutout (a) experiment, (b) simulation.

Figure 17 shows the deformed shape of the joint near the cutout, from both experiment and simulation. While the shape appears to be mostly similar, thus further validating the numerical results, some differences can be noted. For example, the strips of material between the cutouts develop an inward buckled shape in the experiment, while the simulation does not develop the same behavior. This is most visible in the center strip, pointed with red arrows in Figs. 17(a) - 17(b), and it occurs because of a slight shape imperfection of the mold used to build the joint, which creates a localized, concave bend at the joint intersection.

VIII. Summary and Comparison of Results

Different joint designs obtained via physical intuition, parametric optimization, and level-set method were presented. A summary of bending stiffness and norm of first failure index for the various designs is provided in Table 3 and shown in Fig. 18. The most desirable design would populate the upper left corner of the plot, thus providing high bending

stiffness and low failure index norm. Unfortunately, when the bending stiffness of the deployed joint increases, the joint is also more likely to fail when folded and vice versa.

Table 3 Summary of bending stiffness and norm of first failure index values of joint designs studied in the paper. The corresponding joint designs are shown in Fig. 18.

	Name	Norm $\|FI_1\|_2$	Stiffness [Nmm]
Intuitive	A_1	36.7	2310.6
	A_2	55.0	1713.4
	A_3	47.8	1228.7
	A_4	4.68	995.70
Optimized	B_1	19.7	1148.2
	B_2	23.9	2202.2
	B_3	40.9	3137.8
	B_4	26.2	2525.4

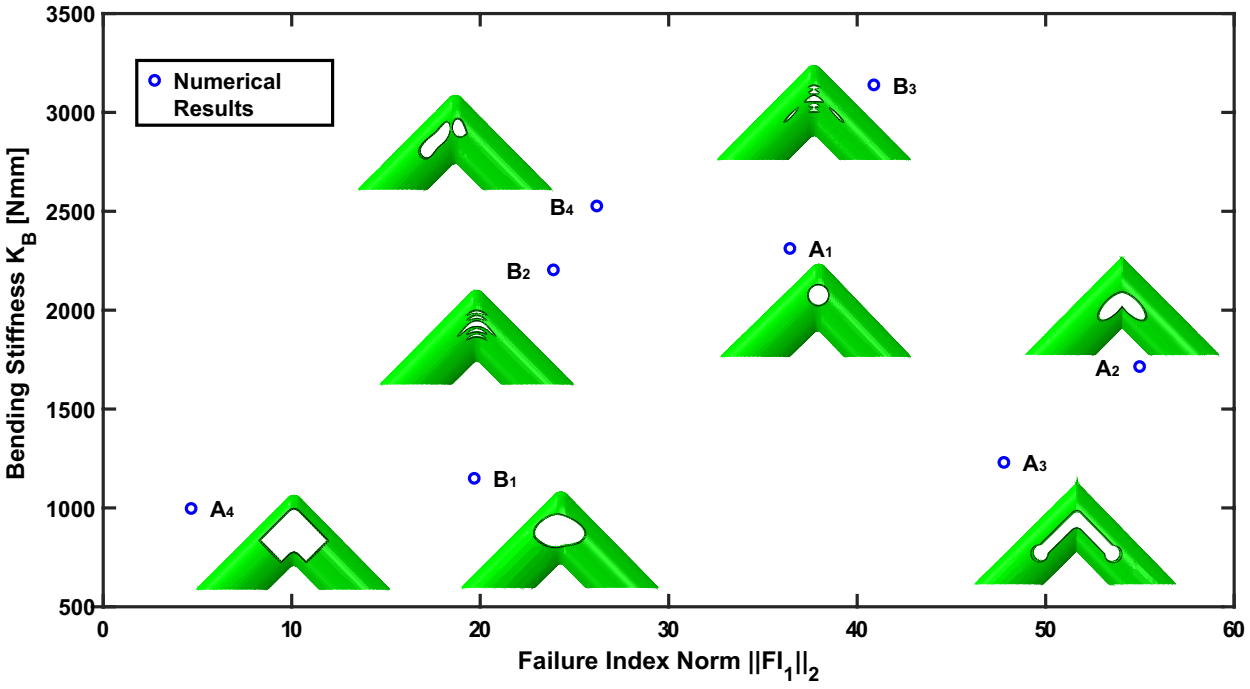

Fig. 18 Numerical results of deployed bending stiffness plotted against $\|FI_1\|_2$ and joint designs studied in the paper.

Two results obtained using physical intuition, A_2 and A_3, have bending stiffness lower than 2000 Nmm and norm of failure index higher than 45. This is partially due to the fact that these designs have sharp corners, which contribute to cause failure. The design named A_4 adopts smooth corners and much larger cutouts. This solution drastically reduced $\|FI_1\|_2$, but suffered a substantial penalty in bending stiffness. The circular cutout, A_1, has much higher bending stiffness, but also higher failure index norm. This resulted in failure of large areas of the joint, Fig 3. Parametric

optimization studies produced a new design, B_1, which reduced the areas on the joint that do not satisfy the failure criterion to a few, concentrated elements. Nevertheless, the cutouts spanned through part of the four-ply region, thus sacrificing bending stiffness. This detail can be improved by adding more control points. Finally, three resulting designs from the level-set method are also plotted. Amongst these, the design named B_2 is the most promising one, since it provides the lowest failure index norm of the three. In fact, a physical joint with this design was tested, Section VII.C, and showed no signs of global failure. Although the result from the level-set method named B_3 shows a much higher failure index norm than the one named B_4, one can also see that a much larger area on B_4 fails, Fig. 15, if compared to B_3, Fig. 14. This indicates that the area that fails is another important parameter that needs to be considered.

Table 4 Mesh convergence studies on joint B_2 with S3 shell elements.

Mesh Size [mm]	Stiffness [Nmm]	Norm $\|\|FI_1\|\|_2$	Max FI_1	Area with $FI_1 > 1$ [mm^2]	Elements with $FI_1 > 5$
2	2281	23.85	9.379	65.81	3
1	2188	38.02	8.679	36.82	4
0.5	2135	70.03	11.768	24.20	9
0.25	2111	132.76	22.513	16.14	31
0.125	2105	159.60	19.643	13.68	66
0.0625	2103	232.08	20.934	12.13	171

A mesh convergence study on joint B_2 was performed to understand the relationship between global/localized failure and the numerical results showing larger or smaller areas on the joint that do not satisfy the failure criterion. The results are shown in Table 4. It is clear that a smaller mesh produces higher values of $\|FI_1\|_2$, while the overall area that fails becomes smaller. To interpret this result, the number of elements with first failure index value bigger than 1 was also provided. As the area that fails gets smaller, a larger number of elements reaches higher values of first failure index. Physically, this correspond to a localization of failure, which is better captured with a smaller mesh. The norm of the first failure index also becomes much larger because of the increased number of elements with high failure index values. Figure 19(a) shows the contour plot of the first failure index on joint B_2 for an average mesh size of 0.0625 mm. The total area that fails measures 12.13 mm^2. The finite element analysis that produced the contour plot reached numerical convergence, thus suggesting this is not a numerical artifact. Additionally, the moment-rotation curves in Fig. 19(b) show that mesh convergence was reached.

IX. Discussion and Conclusion

This study has developed a novel level-set method for optimizing the topology of composite, thin-shells with geometrical non-linearities. This fills a gap in existing topology optimization methods, which do not provide examples of concurrent optimization of structures made of thin composite materials, analyzed with shell elements, and undergoing

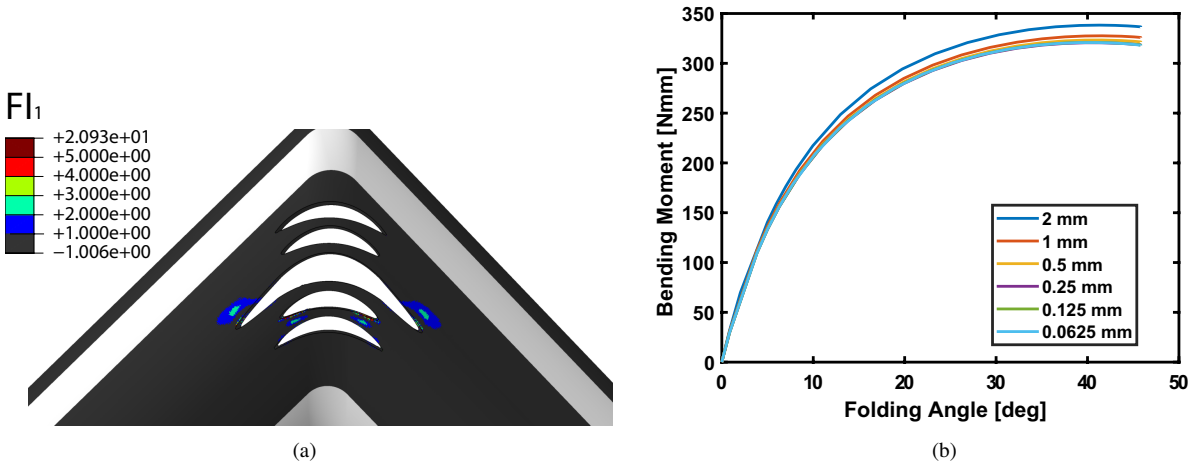

Fig. 19 Analysis of localized failure of joint B_2 (a) contour plot of FI_1 for a mesh size of 0.0625 mm, (b) moment-rotation plots obtained from finite element simulations with different mesh sizes.

large displacements. The validity of the method was demonstrated for the design of self-deployable joints and results were compared to joint designs obtained using physical intuition and parametric optimization. One considerable advantage of the level-set method presented here is the drastic reduction of the number of design variables needed to obtain a good variety of solutions, if compared to the parametric optimization approach.

Almost all the joint designs presented in this study, with the exception of A_4, do not satisfy everywhere the failure criterion. Nevertheless, an important difference between the optimized joint designs and most of the intuitive ones is that the area of the joint that fails, and experimentally defined by visible cracks occurring during folding experiments and a change in bending stiffness of the joint before and after folding, is very much larger for joints A_1, A_2, and A_3. Figure 3 shows large areas that fail on a joint with circular cutouts, which correspond experimentally to large cracks (more than 5 mm long) forming on the sides of the cutouts when the joint is folded [8]. In contrast, Fig. 19 shows only small parts of the joint violating the failure criterion, which correspond experimentally to no signs of visible cracks on a folded joint and no change in bending stiffness, Section VII.C.

While numerical, localized failure is detected, further studies are needed to understand whether the joint actually fails. In fact, the experiments conducted so far, Section VII.C, do not allow to detect localized failure such as fibers microbuckling [26]. Additionally, size scaling effects on the strength of fiber-reinforced composites [30, 31] suggest that the nominal strength of composite laminates, σ_N, including plain weave laminates, increases as the representative size of the test sample, d, decreases. These results can be described by the equation:

$$\sigma_N = f_r^0 \left(1 + \frac{r d_b}{d}\right)^{1/r} \tag{8}$$

Where f_r^0 is the average tensile strength of a boundary layer, which develops at the tensile face of a sample tested in

bending and is a property of the fiber composite, and is considered to be constant; r is a positive constant signifying a transition slowness parameter; d_b is half the thickness of the boundary layer; d is the representative size of the test sample. According to this formula, composite samples tested in bending with smaller representative size will return higher strength values than larger samples. Since the joint design under study, B_2, develops very localized failure, these scaling effects might have to be considered.

Acknowledgments

This work was supported by a NASA Space Technology Research Fellowship. S.F. would like to acknowledge the mentorship of Dr. William Doggett, NASA Langley, and Thibaud Talon, Caltech, for exchange of ideas.

References

[1] Pellegrino, S., Kebadze, E., Lefort, T., and Watt, A., *Low-cost hinge for deployable structures*, University of Cambridge, Department of Engineering, CUED/D-STRUCT/TR202, 2002.

[2] Footdale, J., Banik, J., and Murphey, T., "Design developments of a non-planar deployable structure," *51st AIAA/ASME/ASCE/AHS/ASC Structures, Structural Dynamics, and Materials Conference 18th AIAA/ASME/AHS Adaptive Structures Conference 12th*, 2010, p. 2608.

[3] Francis, W., Lake, M., Mallick, K., Freebury, G., and Maji, A., "Development and testing of a hinge/actuator using elastic memory composites," *44th AIAA/ASME/ASCE/AHS/ASC Structures, Structural Dynamics, and Materials Conference*, 2003, p. 1496.

[4] Barrett, R., Francis, W., Abrahamson, E., Lake, M., and Scherbarth, M., "Qualification of elastic memory composite hinges for spaceflight applications," *47th AIAA/ASME/ASCE/AHS/ASC Structures, Structural Dynamics, and Materials Conference 14th AIAA/ASME/AHS Adaptive Structures Conference 7th*, 2006, p. 2039.

[5] Mobrem, M., and Adams, D., "Lenticular jointed antenna deployment anomaly and resolution onboard the Mars Express spacecraft," *Journal of Spacecraft and Rockets*, Vol. 46, No. 2, 2009, pp. 403–410.

[6] Mallikarachchi, H., and Pellegrino, S., "Quasi-static folding and deployment of ultrathin composite tape-spring hinges," *Journal of Spacecraft and Rockets*, Vol. 48, No. 1, 2011, pp. 187–198.

[7] Hogstrom, K., and Pellegrino, S., "Methods for Characterizing the Reliability of Deployable Modules for Large Optical Reflectors," *3rd AIAA Spacecraft Structures Conference*, 2016, p. 2164.

[8] Ferraro, S., and Pellegrino, S., "Self-Deployable Joints for Ultra-Light Space Structures," *2018 AIAA Spacecraft Structures Conference*, 2018, p. 0694.

[9] Tan, L. T., and Pellegrino, S., "Thin-shell deployable reflectors with collapsible stiffeners Part 1: approach," *AIAA journal*, Vol. 44, No. 11, 2006, pp. 2515–2523.

[10] Mallikarachchi, H., and Pellegrino, S., "Optimized Designs of Composite Booms with Tape Spring Hinges," *51st AIAA/ASME/ASCE/AHS/ASC Structures, Structural Dynamics, and Materials Conference 18th AIAA/ASME/AHS Adaptive Structures Conference 12th*, 2010, p. 2750.

[11] Bendsoe, M. P., and Sigmund, O., *Topology optimization: theory, methods, and applications*, Springer Science & Business Media, 2013.

[12] Andreassen, E., Clausen, A., Schevenels, M., Lazarov, B. S., and Sigmund, O., "Efficient topology optimization in MATLAB using 88 lines of code," *Structural and Multidisciplinary Optimization*, Vol. 43, No. 1, 2011, pp. 1–16.

[13] Sigmund, O., and Maute, K., "Topology optimization approaches," *Structural and Multidisciplinary Optimization*, Vol. 48, No. 6, 2013, pp. 1031–1055.

[14] Wang, M. Y., Wang, X., and Guo, D., "A level set method for structural topology optimization," *Computer methods in applied mechanics and engineering*, Vol. 192, No. 1-2, 2003, pp. 227–246.

[15] Bruns, T. E., and Tortorelli, D. A., "An element removal and reintroduction strategy for the topology optimization of structures and compliant mechanisms," *International journal for numerical methods in engineering*, Vol. 57, No. 10, 2003, pp. 1413–1430.

[16] Wang, F., Lazarov, B. S., Sigmund, O., and Jensen, J. S., "Interpolation scheme for fictitious domain techniques and topology optimization of finite strain elastic problems," *Computer Methods in Applied Mechanics and Engineering*, Vol. 276, 2014, pp. 453–472.

[17] Cho, S., and Jung, H.-S., "Design sensitivity analysis and topology optimization of displacement–loaded non-linear structures," *Computer Methods in Applied Mechanics and Engineering*, Vol. 192, No. 22-24, 2003, pp. 2539–2553.

[18] Pedersen, C. B., Buhl, T., and Sigmund, O., "Topology synthesis of large-displacement compliant mechanisms," *International Journal for numerical methods in engineering*, Vol. 50, No. 12, 2001, pp. 2683–2705.

[19] Pedersen, C. B., Bose, K., Wood, M., Fan, R., and Belsky, V., "Latest Developments for Industrial Adjoint Sensitivity Analysis and Non-Parametric Optimization," 2017.

[20] Ye, Q., Guo, Y., Chen, S., Lei, N., and Gu, X. D., "Topology optimization of conformal structures on manifolds using extended level set methods (X-LSM) and conformal geometry theory," *Computer Methods in Applied Mechanics and Engineering*, Vol. 344, 2019, pp. 164–185.

[21] Sigmund, O., and Torquato, S., "Composites with extremal thermal expansion coefficients," *Applied Physics Letters*, Vol. 69, No. 21, 1996, pp. 3203–3205.

[22] Sigmund, O., "A new class of extremal composites," *Journal of the Mechanics and Physics of Solids*, Vol. 48, No. 2, 2000, pp. 397–428.

[23] Andreassen, E., and Andreasen, C. S., "How to determine composite material properties using numerical homogenization," *Computational Materials Science*, Vol. 83, 2014, pp. 488–495.

[24] Ning, X., and Pellegrino, S., "Design of lightweight structural components for direct digital manufacturing," *53rd AIAA/ASME/ASCE/AHS/ASC Structures, Structural Dynamics and Materials Conference 20th AIAA/ASME/AHS Adaptive Structures Conference 14th AIAA*, 2012, p. 1807.

[25] Mallikarachchi, H., and Pellegrino, S., "Failure criterion for two-ply plain-weave CFRP laminates," *Journal of Composite Materials*, Vol. 47, No. 11, 2013, pp. 1357–1375.

[26] Fleck, N., and Budiansky, B., "Compressive failure of fibre composites due to microbuckling," *Inelastic deformation of composite materials*, Springer, 1991, pp. 235–273.

[27] Wales, D. J., and Doye, J. P., "Global optimization by basin-hopping and the lowest energy structures of Lennard-Jones clusters containing up to 110 atoms," *The Journal of Physical Chemistry A*, Vol. 101, No. 28, 1997, pp. 5111–5116.

[28] Li, Z., and Scheraga, H. A., "Monte Carlo-minimization approach to the multiple-minima problem in protein folding," *Proceedings of the National Academy of Sciences*, Vol. 84, No. 19, 1987, pp. 6611–6615.

[29] Powell, M. J., "A direct search optimization method that models the objective and constraint functions by linear interpolation," *Advances in optimization and numerical analysis*, Springer, 1994, pp. 51–67.

[30] Jackson, K. E., "Scaling effects in the flexural response and failure of composite beams," *AIAA journal*, Vol. 30, No. 8, 1992, pp. 2099–2105.

[31] Bažant, Z. P., Zhou, Y., Novák, D., and Daniel, I. M., "Size effect on flexural strength of fiber-composite laminates," *Journal of Engineering Materials and Technology, Transactions of the ASME*, Vol. 126, No. 1, 2004, pp. 29–37.